Helmholtz-Zentrum Dresden-Rossendorf (HZDR)

HELMHOLTZ ZENTRUM
DRESDEN ROSSENDORF

Unraveling carrier's kinetics in tuning the ferromagnetism of transparent Zn0.95Co0.05O epitaxial films

Satyarthi, P.; Ghosh, S.; Sekhar, B. R.; Wang, Y.; Zhou, S.; Skorupa, I.; Bürger, D.; Schmidt, H.; Srivastava, P.;

Originally published:

June 2016

Journal of Alloys and Compounds 687(2016), 28-36

DOI: https://doi.org/10.1016/j.jallcom.2016.06.082

Perma-Link to Publication Repository of HZDR:

https://www.hzdr.de/publications/Publ-23961

Release of the secondary publication
on the basis of the German Copyright Law § 38 Section 4.

CC BY-NC-ND

Accepted Manuscript

Unraveling carrier's kinetics in tuning the ferromagnetism of transparent $Zn_{0.95}Co_{0.05}O$ epitaxial films

P. Satyarthi, S. Ghosh, B.R. Sekhar, Y. Wang, S. Zhou, I. Skorupa, D. Bürger, H. Schmidt, P. Srivastava

PII: S0925-8388(16)31806-0

DOI: 10.1016/j.jallcom.2016.06.082

Reference: JALCOM 37951

To appear in: *Journal of Alloys and Compounds*

Received Date: 15 March 2016

Revised Date: 31 May 2016

Accepted Date: 9 June 2016

Please cite this article as: P. Satyarthi, S. Ghosh, B.R. Sekhar, Y. Wang, S. Zhou, I. Skorupa, D. Bürger, H. Schmidt, P. Srivastava, Unraveling carrier's kinetics in tuning the ferromagnetism of transparent $Zn_{0.95}Co_{0.05}O$ epitaxial films, *Journal of Alloys and Compounds* (2016), doi: 10.1016/j.jallcom.2016.06.082.

This is a PDF file of an unedited manuscript that has been accepted for publication. As a service to our customers we are providing this early version of the manuscript. The manuscript will undergo copyediting, typesetting, and review of the resulting proof before it is published in its final form. Please note that during the production process errors may be discovered which could affect the content, and all legal disclaimers that apply to the journal pertain.

ACCEPTED MANUSCRIPT

Unraveling carrier's kinetics in tuning the ferromagnetism of transparent $Zn_{0.95}Co_{0.05}O$ epitaxial films

P. Satyarthi[a], S. Ghosh[a, *], B.R. Sekhar[b], Y. Wang[c], S. Zhou[c], I. Skorupa[c,d], D. Bürger[d], H. Schmidt[d], and P. Srivastava[a]

[a]*Nanostech Laboratory, Department of Physics, Indian Institute of Technology Delhi, Hauz Khas, New Delhi 110016, India*

[b]*Institute of Physics, Bhubaneswar 751005, India*

[c]*Helmholtz-Zentrum Dresden-Rossendorf, Institute of Ion Beam Physics and Materials Research, Bautzner Landstr. 400, 01328 Dresden, Germany*

[d]*Department of Materials for Nanoelectronics, Chemnitz University of Technology, 09126 Chemnitz, Germany*

Abstract: The search of transparent conducting and ferromagnetic properties in $Zn_{1-x}Co_xO$ based diluted magnetic semiconductor is explored either by chemically alloying the different concentration (x) of Co or by n-type co-doping. The present work aims to explore the electrical conduction process at variable temperatures, in order to probe the room and low temperature ferromagnetism triggered in transparent $Zn_{0.95}Co_{0.05}O$ films using inert xenon ion irradiation. The origin of the paramagnetism and the tunable ferromagnetism in transparent $Zn_{0.95}Co_{0.05}O$ films is explained from different degree of concentric bound magnetic polarons (BMPs) stabilization inside variable range hopping spheres through implication of strongly and weakly bound carriers to O/Zn related lattice defects and tetrahedrally substituted Co^{2+} ions. The paramagnetic behavior in as deposited $Zn_{0.95}Co_{0.05}O$ film arises from the smallest density of isolated concentric BMPs resulted mainly from marginal concentration of strongly localized carrier due to its highly insulating nature. The progressive enhancement in strongly localized carriers in post irradiated $Zn_{0.95}Co_{0.05}O$ films as a function of fluence results in overlapping of static concentric BMPs to trigger onset of ferromagnetism. The strength of ferromagnetism is found to be maximal at a particular density of concentric BMPs optimized from the highest concentration of strongly localized carriers in insulating regime and substantial substituted Co^{2+} ions. Further enhancement in carrier concentration and reduction in substituted Co^{2+} ions is detrimental to ferromagnetism owing to non-static concentric BMPs percolation from the presence of weakly localized nature of carriers in intermediate regime.

* **Corresponding author (e-mail: santanu1@physics.iitd.ac.in)**

1. Introduction

In the last decade, diluted magnetic semiconductors (DMSs) [1,2] and transparent conductors [2,3] have attracted much attention because of their potential applications in the fields of spintronics and optoelectronics [4,5]. However, for the development of next generation opto-spintronic devices, such as spin-LED (light emitting diode), spin-RTD (resonant tunneling devices), and optical switches; optoelectronic and ferromagnetic properties should coexist in the same host matrix. In this regard, zinc oxide (ZnO) is one of the most favorable host materials due to its large optical band gap (~ 3.3 eV) and intrinsic n-type characteristics from Zn/O related interstitial and vacancy defects [5,6]. A fairly large number of studies have aimed to investigate transparent conducting and ferromagnetic properties in ZnO by doping it with transition metal elements including Fe, Co, Ni and Cu [7-13]. In particular, $Zn_{1-x}Co_xO$ has shown strong potential from the perspective of both properties [8,9,11]. However, it is also reported that optical properties such as transmittance and band gap are greatly reduced as a function of Co concentration in ZnO matrix [14], which is not desirable for potential transparent conductors. Apart from questions related to the optical properties, origin of conductance and ferromagnetic ordering in $Zn_{1-x}Co_xO$ based DMSs remains inconclusive, as Co dopants and carriers can play an active as well as passive role. In majority of the studies, Co dopants in ZnO matrix have segregated as metallic Co or intermetallic ZnCo clusters [15-17], to trigger extrinsic ferromagnetism (FM), which is detrimental to spintronic applications. However, the substitution of Co dopants in regular crystallographic structure of ZnO dominates intrinsic FM [18-20], which is within the frame work of free carrier mediated exchange interaction [7,19] and bound carrier constituted magnetic polarons (BMPs) formation [18-20]. Of late, attempts have been made to further enhance the conducting properties in $Zn_{1-x}Co_xO$ based DMSs by codoping it with

donor type elements like Al [19,21,22] and Ga [23], and explore the kinetics of charge carriers in relation to FM. Majority of the studies have reported that intrinsic FM is stabilized in $Zn_{1-x}Co_xO$:Al/Ga films when the carrier concentration lies in insulating and metallic regime which is consistent with BMP [19,20,23] and carrier mediated [19,23] mechanisms respectively. However, decrease/lack of FM is seen for carrier concentration lying in intermediate regime [19,23]. Very surprisingly, absence of FM is also cited in metallic $Zn_{1-x}Co_xO$:Al films [21,22] despite the presence of very high carrier concentration, which has raised serious doubt over the role of carriers generated by donors like Al and Ga. Ion implantation/irradiation has been established as another effective method for the generation of O vacancies and Zn interstitials defects [24,25] in ZnO in a controlled manner, which in turn act as source of n-type carriers for FM. In addition, in the recent past there has been an emerging consensus over the vital role of Zn/O related defects in origin of d^0 FM for undoped ZnO systems [25-27] which indicate that FM may not be exclusively correlated to the presence of transition metal, but also mediated by inherently present or intentionally induced Zn/O related lattice defects. The generation and organization of defects in $Zn_{1-x}Co_xO$ matrix through post ion implantation/irradiation which may control n-type carriers are an important issue and needs further exploration.

In the existing literature, there has been a great deal of interest on search of transparent conducting and ferromagnetic properties in $Zn_{1-x}Co_xO$ based DMSs by codoping n-type donors of various concentration. However, the role of n-type donors in relation to presence/absence of FM remains equally controversial. The present work originates with motivation to highlight the importance of inert xenon (Xe) ion irradiation for tuning the transparent conducting and ferromagnetic properties in $Zn_{0.95}Co_{0.05}O$ films even without adding any n-type dopants. In the recent works [28,29], the lack/presence of room temperature ferromagnetism (RT-FM) in as

deposited/post irradiated $Zn_{0.95}Co_{0.05}O$ films has been correlated with their electronic and local structure. However, it is extremely important to understand the electrical conduction and transmittance of these ferromagnetic films, before implementing them for any device fabrication in future opto-spintronics. Motivated by this, a systematic study on electrical conduction process of as deposited and post irradiated $Zn_{0.95}Co_{0.05}O$ films at variable temperature (down to 5 K) is the prime focus of the present study. An attempt has been made to correlate the electrical transport with the transmittance and ferromagnetism at room (300 K) and low (5 K) temperature in these $Zn_{0.95}Co_{0.05}O$ films, by proposing a modified BMPs model based on concentric BMPs spheres constituted by strongly/weakly bound carriers and substituted Co^{2+} ions.

2. Experimental details

The 5 at. % Co doped ZnO films ($Zn_{0.95}Co_{0.05}O$) of thickness ~ 200 nm were grown on sapphire substrate by pulsed laser deposition (PLD) technique using a KrF excimer laser. During the deposition, the oxygen partial pressure and substrate temperature were kept at 6.5×10^{-3} mbar and 550 ^{o}C respectively [28,29]. As deposited $Zn_{0.95}Co_{0.05}O$ films were irradiated at RT with 500 keV inert Xe^{3+} ions using the low energy ion beam facility (LEIBF) [30] of the Inter University Accelerator Centre, New Delhi, India. In the LEIBF facility, a fully permanent magnet based electron cyclotron resonance ion source operating at 10 GHz frequency was placed on high voltage platform (0-400 KeV) to produce stable Xe ion beam. The Xe ion beam of 1 μA current was scanned horizontally and vertically on the as-deposited $Zn_{0.95}Co_{0.05}O$ films mounted in evacuated chamber for uniform irradiation. The different ion fluences (5×10^{14}, 1×10^{16}, 5×10^{16} and 1×10^{17} ions/cm^2) of incident Xe beam were used to tune the defect density by ion-materials interaction. The range (~ 100 nm) and longitudinal straggling distribution (~ 29 nm) of the 500 keV ions in $Zn_{0.95}Co_{0.05}O$ films have been calculated using the simulation program Transport of

Ions in Matter (TRIM) [31]. The structural characterization of as deposited and post irradiated $Zn_{0.95}Co_{0.05}O$ films were carried out at RT using x-ray diffraction (XRD) (Philips X'Pert PRO) with CuK_α radiation (λ = 0.1542 nm). Chemical state and defect chemistry of different elements present in these $Zn_{0.95}Co_{0.05}O$ films were analyzed by x-ray photoelectron spectroscopy (XPS) (SPECS) using MgK_α source (hv = 1253.6 eV) in a base pressure below 1×10^{-9} mbar. Ultraviolet/visible (UV-Vis) spectroscopy (UV 3600: Shimazdu) was used to determine the optical transmittance of the films. Electrical transport including Hall measurements at room temperature were carried out for as deposited and post irradiated $Zn_{0.95}Co_{0.05}O$ films using metallic contacts in van der Pauw configuration. The electrical resistivity as a function of temperature was also measured for these films in the temperature range from 5 K to 300 K using linear four probe method. For carrying out the measurements, the film was kept in evacuated chamber, which was cryogenically cooled down to 5 K. The temperature controller (Lake Shore) and source meter (Keithley) were used to measure the temperature and resistance respectively. The magnetic properties of these $Zn_{0.95}Co_{0.05}O$ films were investigated using a vibrating sample (VSM) magnetometer (Quantum design).

3. Results and discussion

The XRD patterns of as deposited and post irradiated $Zn_{0.95}Co_{0.05}O$ films showed wurtzite structure with a preferred orientation along the c-axis and was reported earlier [28]. Any diffraction peak associated with secondary phases of crystalline Zn metal and Co metal or CoO was not detected within the detection limit of XRD. From XRD measurements, it is difficult to get any information related to the presence of any amorphous phase of Zn metal and Co metal or its oxide Therefore, XPS and optical transmittance measurements have been employed to

ascertain the oxidation state and structural environment of constituents in as deposited and post irradiated $Zn_{0.95}Co_{0.05}O$ films.

3.1. X-ray photo emission studies of $Zn_{0.95}Co_{0.05}O$ films

The Zn 2p core level photoemission spectra of as deposited and post irradiated $Zn_{0.95}Co_{0.05}O$ films are shown in Fig. 1. In as deposited and lowest fluence (5×10^{14} ions/cm^2) irradiated $Zn_{0.95}Co_{0.05}O$ films, the binding energy (B. E.) of Zn $2p_{3/2}$ and Zn $2p_{1/2}$ peaks are observed around 1021.9 eV and 1044.9 eV respectively with a spin-orbit splitting of 23 eV, which matches closely with the binding energy values (1022 eV and 1045 eV) of Zn^{2+} ions in ZnO [25,32,33]. It confirms that Zn atoms are in +2 oxidation state in tetrahedral wurtzite environment and any possibility of interstitial metallic Zn (1021.5 eV) and Zn vacancy is excluded [32,33]. However, the binding energy of Zn $2p_{3/2}$ and Zn $2p_{1/2}$ peaks in the films irradiated at higher fluences (1×10^{16} ions/cm^2 and higher) shifts slightly to lower energy side at ~ 1021.7 eV and ~ 1044.7 eV respectively (see the dotted line), which can be interpreted to be caused by an enhancement in effective electron density of Zn atoms from the presence of small fraction of Zn interstitials (Zn_i) in addition to predominant Zn^{2+} ions. The presence of Zn_i defects suggests the formation of Zn vacancy defect, which was also evident in x-ray absorption near and far edge structure (XANES and EXAFS) analysis at *K*-edges of Zn and Co [28,29]. These Zn_i and Zn vacancy related defects are triggered by the dense collision cascade developed inside the $Zn_{0.95}Co_{0.05}O$ matrix by nuclear energy loss mechanism (3.8×10^2 eV/Å calculated from TRIM) of 500 keV xenon ions with target Zn atoms at regular wurtzite sites [29,34,35].

Fig. 2 shows a typical O 1s core level spectra corresponding to as deposited $Zn_{0.95}Co_{0.05}O$ film. The broad and asymmetric nature of peak indicate multi component of oxygen, which can be fitted into three Gaussian peaks having different binding energy components at 530.3 eV, 531.2

eV, and 532.4 eV respectively [28,36,37]. The dominant peak (O_I) centered at lower binding energy side (530.3 eV) of the O 1s spectrum is associated with O^{2-} ions in wurtzite structure of hexagonal Zn^{2+} ion array. The peak marked as O_{II} for binding energy of 531.2 eV is attributed to oxygen ions in oxygen deficient regions within the ZnO matrix [28,36]. The relative area under this peak is an indication of oxygen vacancies, which is in general lower than the O_I component. The higher binding energy component (O_{III}) is usually due to the presence of loosely bound oxygen on the surface of film, attached with specific species such as -CO_3, absorbed H_2O, or absorbed O_2 [28,37]. The relative area of O_I, O_{II} and O_{III} peaks for all post irradiated $Zn_{0.95}Co_{0.05}O$ films is calculated from their O 1s spectra (plots not shown) to extract information for relative area of O_{II} peak, which is shown in inset of Fig. 2. It is evident from the inset of Fig. 2 that relative area of oxygen vacancies increases as the irradiation fluence increases and it gets maximized at intermediate fluence. The enhancement of anionic vacancy related defects in post irradiated $Zn_{0.95}Co_{0.05}O$ films is again understood from the dense collision cascades as a result of interaction between high energetic Xe ions and anions at regular wurtzite sites.

The Co 2p core level photo emission spectra for as deposited and post irradiated $Zn_{0.95}Co_{0.05}O$ films are shown in Fig. 3. The spectra of these films show four peaks corresponding to the $2p_{3/2}$ and $2p_{1/2}$ core levels and their shake-up resonance transitions (satellite) at higher binding energy [14,32]. It is to be emphasized that within the detection limit of XPS, the signal to noise ratio in Co 2p core level spectra is not so good as in Zn 2p and O 1s core level spectra, due to low content (5 at. %) of Co. However, the binding energy of $2p_{3/2}$ (780.5 ±0.1 eV) and $2p_{1/2}$ (796.1 ±0.1 eV) core levels as well as energy difference (15.6 ±0.1) between two matches closely with Co^{2+} oxidation state in Co-O bonding. There is no indication of peaks at 778 and 793 eV corresponding to metallic Co for as deposited and post irradiated films [14]. It suggests that

majority of the Co dopants incorporate in wurtzite lattice as Co^{2+} ions for as deposited and irradiated films. The electronic structure of Co dopants as discussed above provide a qualitative picture, as low fraction of Co dopants is present within probing depth (20-40 Å) of XPS. In order to get better insight for the oxidation state of Co dopants and their crystallographic environment in the whole volume of films, optical absorption measurements are discussed below.

3.2. Optical properties of $Zn_{0.95}Co_{0.05}O$ films

Optical transmittance spectra of as deposited and post irradiated $Zn_{0.95}Co_{0.05}O$ films are shown in Fig. 4. The spectra reveal strong decrease in transmittance at the band gap energy and three absorption edges located at 1.88 eV (A), 2.01 eV (B) and 2.20 eV (C). In the literature [8,14], these edges (A, B and C) are correlated to d-d transitions of Co^{2+} ions substituted at Zn^{2+} sites in tetrahedral crystal field of ZnO and can be attributed to $^4A_2(F) \rightarrow {}^2E(G)$, $^4A_2(F) \rightarrow {}^4T_1(P)$ and $^4A_2(F) \rightarrow {}^2A_1(G)$ transitions respectively. The intensity of these absorption edges is found to be proportional to the concentration of substituted Co^{2+} ions, if there is no variation in film thickness. It is interesting to note that intensity of different absorption edges as well as transmittance decreases at higher fluences although Co concentration is same in all the films. It strongly suggests that for as deposited and irradiated films corresponding to 5×10^{14} and 1×10^{16} ions/cm^2 fluences, majority of the Co dopants have substituted the Zn^{2+} ions in tetrahedral crystal field of ZnO, which results in higher transmittance ($\geq$ 90 %). However due to significant reduction in the percentage of substituted Co^{2+} ions, as evident from the absorption edges, decrease in transmittance (~ 40-43 %) is seen for films irradiated at higher fluences (5×10^{16} and 1×10^{17} ions/cm^2). There may be a possibility of a small fraction of Co atoms residing either on

random interstitial sites as metallic Co or in some other non-wurtzite environment particularly for these two films.

3.3. Transport properties of $Zn_{0.95}Co_{0.05}O$ films

The results obtained from resistivity and Hall effect measurements at room temperature for the as deposited and post irradiated $Zn_{0.95}Co_{0.05}O$ films reveal n-type conduction and data of resistivity (ρ), carrier concentration (n_c) and Hall mobility (μ) are depicted in Fig. 5. It is evident that resistivity decreases appreciably in post irradiated films as a function of fluence, which is due to increase in carrier concentration and Hall mobility. The resistivity decreases rapidly for the film irradiated at intermediate fluence (5×10^{16} ions/cm^2). The change in resistivity and carrier concentration can be attributed to O/Zn related vacancy and interstitial defects generated due to Xe ion irradiation. It is to be emphasized the carrier concentration for the film irradiated at 5×10^{16} ions/cm^2 fluence is found to be close to free carrier concentration ($\geq 1\times10^{20}$ cm^{-3}) required for metallic conduction [19,22]. Therefore to examine the type of conduction in all films, detailed resistivity versus temperature measurements are discussed for the two representative irradiated films corresponding to fluences of 1×10^{16} and 5×10^{16} ions/cm^2.

Fig. 6 shows the temperature dependent electrical resistivity for the films irradiated at the fluences of 1×10^{16} and 5×10^{16} ions/cm^2. Both the films reveal $d\rho/dT < 0$ in whole temperature range of 5-300 K, which rules out the possibility of metallic conduction in both films. It is to be noted that resistivity increases strongly at lower temperatures for the film irradiated with 1×10^{16} fluence. The strong dependence of resistivity on temperature suggests the insulating behavior for this film. In insulating regime, carriers (electrons) tend to be strongly localized at defects and they can hop from one site to another under specific probability. However, for the film irradiated with 5×10^{16} fluence, there is a slight increase in resistivity with decreases in temperature. The

weak temperature dependence of resistivity for this film suggests the intermediate regime between metallic and insulating regime. In contrast to the insulating regime, the carriers (electron) in intermediate regime are not so strongly localized at defects and they can hop under favorable condition. Therefore, resistivity versus temperature measurements allow us to conclude that resistivity and carrier concentration of as deposited and lower fluence irradiated films (5×10^{14} and 1×10^{16} ions/cm^2) lie in the insulating regime. However, decreased resistivity, accompanied with increased carrier concentration for films irradiated with 5×10^{16} and 1×10^{17} ions/cm^2 fluences reveals their transport properties corresponding to intermediate regime. Furthermore for both films, the presence of different slopes in resistivity versus temperature curves (see the Fig. 6) shows various mechanisms of carrier transport to be operative in different temperature ranges. According to the existing literature [38-41], around room temperature carriers dominate thermally activated band conduction, whereas at lower temperatures most of the carriers do not have sufficient energy to jump from their donor levels to conduction band. In low temperature regime, they conduct by hopping from one impurity level to another, making the thermally activated band conduction less probable. Because of the hopping of electrons from an occupied level to an empty level, this transport mechanism is classified into two different categories viz. Nearest-Neighbor Hopping (NNH) and Variable Range Hopping (VRH) conduction. In NNH conduction, an electron hops from localized occupied state to the nearest unoccupied state. However in VRH conduction, hopping of electron occurs to those unoccupied states which are near to the Fermi level irrespective of their spatial distribution. In general, it is widely accepted that NNH hopping conduction happens at temperatures lower than 250 K whereas VRH hopping type conduction dominates at much lower temperatures (< 130 K). The thermally activated band conduction, NNH and VRH conduction are discussed below.

The carrier transport in thermally activated band and NNH conduction [40,41] is represented by

$$\sigma = \sigma_1 \exp\left(-\frac{E_{a1}}{kT}\right) + \sigma_2 \exp\left(-\frac{E_{a2}}{kT}\right) \qquad (1)$$

where σ_1 and σ_2 are pre exponential factors, E_{a1} and E_{a2} are activation energies required for band and NNH conduction and k is Boltzmann's constant.

The activation energy required for both conduction is calculated by the Arrhenius plot of ln σ versus 1000/T as shown in Fig. 7 for the irradiated $Zn_{0.95}Co_{0.05}O$ films corresponding to 1×10^{16} ions/cm^2 and 5×10^{16} ions/cm^2 fluences. The activation energy is estimated by the slopes of the curves through best fit technique. The activation energy for band and NNH conduction is found to be 17.9 meV and 9.0 meV respectively for the 1×10^{16} ions/cm^2 irradiated film, whereas these values decrease to 0.54 meV and 0.23 meV respectively for 5×10^{16} ions/cm^2. The rapid decrease in activation energy for 5×10^{16} ions/cm^2 fluence irradiated film is concurrent with enhancement in carrier concentration. The enhancement in carrier concentration raises the Fermi energy to a higher level in the band gap, which in turn leads to decrease in activation energy. It is very likely that for this film, majority of the carriers can do hopping to conducting band and neighboring localized states very easily due to rapid decrease in activation energies.

The carrier transport in low temperature regime can be governed by Mott's VRH model [40-42]

$$\sigma = \sigma_{h0} \exp\left[-\left(\frac{T_0}{T}\right)^{1/4}\right] \qquad (2)$$

where parameters σ_{h0} and T_0 are given by the following expression

$$\sigma_{h0} = \frac{3e^2 v_{ph}}{(8\pi)^{1/2}} \left[\frac{N(E_F)}{\alpha kT}\right]^{1/2}$$

$$T_0 = \left[\frac{16\alpha^3}{kN(E_F)}\right]$$

where ν_{ph} is the phonon frequency (~ 10^{13} Hz) at Debye temperature, k is the Boltzmann's constant, $N(E_F)$ is the density of localized electron states at Fermi level and α is the inverse localization length of the localized state.

Fig. 8 shows the dependence of $\ln(\sigma T^{1/2})$ versus $T^{-1/4}$ for the irradiated $Zn_{0.95}Co_{0.05}O$ films corresponding to 1×10^{16} ions/cm^2 and 5×10^{16} ions/cm^2 fluences. The presence of linear relationship indicates that VRH conduction is operative in the low temperature range. The Mott's variable range hopping parameters ($\sigma_{h0,}$ T_0, $N(E_F)$ and α) obtained from the straight line fitting of $\ln(\sigma T^{1/2})$ versus $T^{-1/4}$ plots are summarized in Table 1. It is evident from the table that density of localized states $N(E_F)$ near the Fermi level is higher for the film irradiated at 5×10^{16} ions/cm^2 fluence as compared to 1×10^{16} ions/cm^2 fluence, which is due to enhanced carrier concentration. In addition, very high value of T_0 for 1×10^{16} ions/cm^2 fluence irradiated film corresponds to low probability of hopping from occupied to unoccupied state and a very high value of resistivity. The inverse localization length parameter α is also large for 1×10^{16} ions/cm^2 fluence as compared to 5×10^{16} ions/cm^2. Accordingly the two important Motts hopping parameters including VRH localization radius ($r_{VRH} = 1/\alpha$) and average hopping jump distance ($R= [9/8\pi\alpha kTN(E_F)]^{1/4}$) are also given in same table [38,39]. The parameter (r_{VRH}) reveals the range of a carrier localized by a defect in its hydrogenic orbit, so called VRH sphere. The parameter (R) denotes the average distance that a carrier can hop out of the VRH sphere. Since the r_{VRH} and R are very high for 1×10^{16} ions/cm^2 fluence irradiated film, which confirm that carriers at defect sites tend to be strongly localized up to a very large distance (~ 23 nm) and there is least probability of hopping of carriers between the two VRH spheres. However for 5×10^{16} ions/cm^2 fluence irradiated film, r_{VRH} and R are relatively less, which confirm that charge carriers become weakly localized to a small distance (~ 6.5 nm) and they hop between VRH

spheres. Therefore it can be concluded that charge carriers for as deposited and lower fluence irradiated films (5×10^{14} and 1×10^{16} ions/cm^2) are strongly localized due to their insulting behavior, however for higher fluence irradiated films (5×10^{16} and 1×10^{17} ions/cm^2), they become weakly localized due to intermediate behavior.

Table 1. The calculated values of Motts's variable range hopping parameters for irradiated $Zn_{0.95}Co_{0.05}O$ films corresponding to 1×10^{16} and 5×10^{16} ions/cm^2 fluences.

Irradiated $Zn_{0.95}Co_{0.05}O$ films	T_0 (K)	α (cm^{-1})	$N(E_F)$ (cm^{-3}eV^{-1})	r_{VRH} (nm)	R (nm)
1×10^{16} ions/cm^2	68000	4.3×10^{7}	2.2×10^{17}	23	52
5×10^{16} ions/cm^2	422	1.5×10^{6}	1.6×10^{21}	6.5	4

3.4. Magnetic properties of $Zn_{0.95}Co_{0.05}O$ films

The magnetization measurements (*M-H*) at room temperature reveal paramagnetic and tunable ferromagnetic behavior for as deposited and post irradiated $Zn_{0.95}Co_{0.05}O$ films respectively, which has been reported in our earlier work [28]. The room temperature saturation magnetization (M_s) of post irradiated $Zn_{0.95}Co_{0.05}O$ films are plotted against carrier concentration (see Fig. 9 (a)). It is interesting to note that M_s is found to be the highest for the irradiated film (1×10^{16} ions/cm^2 fluence) lying in insulating regime. However, reduction in M_s is evident for the irradiated films (5×10^{16} and 1×10^{17} ions/cm^2 fluence) lying in intermediate regime. Moreover, M_s scales with carrier concentration in insulating and intermediate regime. The *M-H* measurements at low temperature (5 K) for irradiated films corresponding to 1×10^{16} and 5×10^{16} ions/cm^2 fluences are presented in Fig 9(b) for understanding the role of carrier kinetics in origin of FM down to low temperature. The room temperature *M-H* data for same films is also presented for the comparison of FM at two temperatures. It is clearly evident that there is an

enhancement in ferromagnetic strength in terms of saturation magnetization, remanent magnetization and coercivity at low temperature *M-H* data. It strongly suggest that carrier mediated exchange interaction cannot be adopted directly to explain FM in these set of films. It appears that an improved BMPs model with specific modification is required to explain FM in insulating and intermediate regime, which is discussed below.

3.5. Role of carrier's kinetics in origin of FM for transparent $Zn_{0.95}Co_{0.05}O$ films

The as deposited film reveals perfect insulating behavior with lowest carrier concentration at room temperature, which arises due to lack of significant Zn/O related lattice defects. However in post irradiated films increasing trend of carrier concentration (at room temperature) is seen due to enhancement of O vacancies and Zn interstitials defects. Furthermore the influence of irradiation is clearly evident in progressive decrease of Co^{2+} ions substitution at Zn^{2+} sites in tetrahedral environment. Although, carrier concentration increases in post irradiated $Zn_{0.95}Co_{0.05}O$ films, but metallic conduction is not evident in any of the irradiated films. Therefore origin of RT-FM in post irradiated $Zn_{0.95}Co_{0.05}O$ films cannot be explained from free carrier mediated exchange interaction, as very high carrier concentration ($\geq 10^{20}$ cm^{-3}) is required in the conduction band to mediated ferromagnetic interaction between Co dopants [19,22]. It is to be emphasized that electrical conductivity in post irradiated $Zn_{0.95}Co_{0.05}O$ films arises from the (i) carriers transport in the conduction band and (ii) carriers hopping within the localized states of Zn/O vacancies and Zn interstitials. At and around room temperature, thermally activated band conduction and hopping mechanism can dominate the conductivity, whereas in low temperatures regime, only hopping conduction contributes. It is reported in literature [39] that for carrier concentration below the ~ 10^{20} cm^{-3}, thermally activated band conduction and hopping conduction coexist in temperature regime of 100-300 K, but the relative proportion of hopping

conduction is always greater than the thermally activated band conduction. However at temperatures below the 100 K, the contribution from thermal activated band conduction ceases to exist and hopping conduction dominates. Therefore, it can be inferred that thermally activated band conduction and hopping conduction can play important roles for understanding the RT-FM of post irradiated $Zn_{0.95}Co_{0.05}O$ films. However, low temperature FM is exclusively correlated to hopping conduction. In case of post irradiated $Zn_{0.95}Co_{0.05}O$ films, it is very unlikely that thermally activated band conduction is solely responsible for inducing spin coherence between the Co dopants to trigger RT-FM due to (i) low content of Co (5 at. %) and (ii) less carrier concentration ($\leq 10^{20}$ cm^{-3}) at room temperature. The presence of very high carrier concentration ($\geq 10^{20}$ cm^{-3}) is required in the conduction band to mediated ferromagnetic interaction between Co dopants of low content (see the Ref. 19, and 22). Therefore, thermally activated band conduction contributes to electrical conductivity predominately in post irradiated $Zn_{0.95}Co_{0.05}O$ films. However hopping conduction at low and high temperatures triggers strong spin coherence between the localized carriers (electrons) at Zn/O defects sites and tetrahedrally substituted Co^{2+} ions to constitute BMPs within a radius (r_{BMP}) of 0.76 nm [20]. Furthermore, these BMPs are formed within the localization radius of carriers so called VRH spheres (6.5 nm - 23 nm) [38], which is schematically depicted in Fig. 10. Therefore formation of BMPs inside the VRH spheres is essential to understand the absence and presence of FM at high and low temperatures, and is discussed below.

It is to be emphasized that for as deposited $Zn_{0.95}Co_{0.05}O$ film, although tetrahedrally substituted Co^{2+} ions is largest but carrier concentration at room temperature is lowest, which in turn results in low density of concentric spheres. Therefore, concentric spheres are distributed far apart and there is no direct interaction between isolated BMPs to give rise to RT-FM in as deposited film.

Therefore paramagnetic behavior is seen in as deposited film, which is pictorially depicted in case I of Fig. 10. However for the $Zn_{0.95}Co_{0.05}O$ films irradiated at lower irradiation fluences (5×10^{14} and 1×10^{16} ions/cm^2), high density of static concentric BMP spheres is favored from the significant concentration of strongly localized carriers and substituted Co^{2+} ions. These static concentric BMPs spheres interact with each other to trigger RT-FM as shown in case II of Fig. 10. The ferromagnetic strength is higher in the film irradiated with 1×10^{16} ions/cm^2 fluence as compared to 5×10^{14} ions/cm^2 fluence due to presence of higher concentration of localized carriers. For the films irradiated at higher fluences (5×10^{16} and 1×10^{17} ions/cm^2), although carrier concentration increases but these tends to be weakly localized due to easily hopping to conduction band and localized states. Furthermore, there is a significant reduction in substituted Co^{2+} ions. It decreases the probability of static concentric BMPs formation within VRH spheres as weakly localized charge carriers can do hopping from their O/Zn related lattice defects sites and hence spin of substituted Co^{2+} ions may also flip due to random electrostatic potential generated by weakly localized carriers (see case III). Therefore, decrease in room temperature saturation magnetization for these irradiated films has been observed as compared to 1×10^{16} ions/cm^2 fluence. The higher saturation magnetization in 5×10^{16} ions/cm^2 fluence as compared to 1×10^{17} ions/cm^2 is again interpreted in terms of higher carrier concentration. It is to be further emphasized that ferromagnetic strength at low temperature *M-H* (5 K) data for irradiated films (1×10^{16} and 5×10^{16} ions/cm^2) enhances in terms of saturation magnetization, remanent magnetization and coercivity. At low temperatures, localization of carriers at defect sites is very strong from the absence of thermally activated band conduction, which in turn stabilizes strong spin coherence between substituted Co^{2+} ions and localized carriers. It gives rise to stable concentric BMPs formation with its enhanced radius inside the VRH sphere. As a result, the

separation between interacting concentric BMPs decreases, therefore, strong magnetic coupling between these results in enhanced ferromagnetic strength. Apart from concentric BMPs, Zn vacancy defects may also be the other possible reason of low and high temperature FM from the spin polarization at unsaturated O 2p orbitals [29,42]. The concentric BMPs formation and Zn vacancy defects are crucial to understand the absence and presence of FM at low and high temperature.

4. Conclusions

In summary, role of carrier's kinetics is explored for understanding the tunable FM induced in as grown $Zn_{0.95}Co_{0.05}O$ transparent films. The origin of the absence/presence of FM in transparent $Zn_{0.95}Co_{0.05}O$ films is understood from the formation of concentric BMPs inside the VRH spheres as a result of strongly and weakly localized carriers bound to Zn/O defect sites and substituted Co^{2+} ions in tetrahedral environment. The paramagnetic behavior of as deposited $Zn_{0.95}Co_{0.05}O$ film is within the framework of smallest density of isolated static concentric BMPs spheres owing to marginal carrier concentration. The enhancement in strongly/weakly localized carriers in post irradiated $Zn_{0.95}Co_{0.05}O$ films as a function of fluence starts the sufficient overlap of concentric BMPs spheres to trigger onset of FM. The strength of FM in post irradiated films is maximized from the percolation of static concentric BMPs as a result of highest concentration of strongly localized carriers in insulating regime and substantial substituted Co^{2+} ions. The further enhancement in carrier concentration and reduction in substituted Co^{2+} ions for the films irradiated at much higher fluences give rise to reduction in FM from the non-static concentric BMPs percolation from weakly localized carriers. These irradiated $Zn_{0.95}Co_{0.05}O$ films with transparent and ferromagnetic properties are potential candidate for different applications in future opto-spintronic devices.

Acknowledgments

We are thankful to Dr. Dinakar Kanjilal and Dr. Pravin Kumar from Inter University Acceleration Centre, India for providing LEIBF facility to conduct for irradiation experiments in $Zn_{0.95}Co_{0.05}O$ epitaxial films. The authors acknowledge Indian Institute of Technology (IIT) Delhi (India) for providing UV-Vis spectroscopy (under high impact research grant of IIT Delhi) and XPS (partially funded by FIST grant of Department of Science & Technology (DST) India) facilities to carry out the optical absorption and electronic structure measurement respectively. Authors, SG and PS acknowledge partial financial support from DST, India. One of the authors (P. Satyarthi) is thankful to University Grant Commission (UGC), India for the financial support through fellowship. IS, DB and HS acknowledge financial support from Deutsche Forschungsgemeinschaft (Bu 2956/1-1, SCHM1663/4-1,2). SZ thanks the Helmholtz-Association for financial support under the project VH-NG-713.

ACCEPTED MANUSCRIPT

References

[1] H. Ohno, Making nonmagnetic semiconductors ferromagnetic, Science 281 (1998) 951-956.

[2] S.J. Pearton, C.R. Abernathy, M.E. Overberg, G.T. Thaler, D.P. Norton, N. Theodoropoulou, A.F. Herbard, Y.D. Park, F. Ren, J. Kim, L.A. Boatner, Wide band gap ferromagnetic semiconductors and oxides, J. Appl. Phys. 93 (2003) 1.

[3] T. Minami, Transparent conducting oxide semiconductors for transparent electrodes, Semincond. Sci. Technol. 20 (2005) S35-S44.

[4] S.A. Wolf, D.D. Awschalom, R.A. Buhrman, J.M. Daughton, S.V. Molnar, M.L. Roukes, A.Y. Chtchelkanova, D.M. Treger, Spintronics: a spin based electronics vision for the future, Science 294 (2001) 1488-1495.

[5] F. Pan, C. Song, X.J. Liu, Y.C. Yang, F. Zeng, Ferromagnetism and possible application in spintronics of transition metal doped ZnO films, Mater. Sci. Eng. R 62 (2008) 1-35.

[6] A. Janotti, C.G.V.D. Walle, Fundamentals of zinc oxide as a semiconductor, Rep. Prog. Phys. 72 (2009) 126501.

[7] K. Ueda, H. Tabata, T. Kawai, Magnetic and electric properties of transition-metal-doped ZnO films, Appl. Phys. Lett. 79 (2001) 988.

[8] S. Ramachandran, A. Tiwari, J. Narayan, $Zn_{0.9}Co_{0.1}O$ based diluted magnetic semiconducting thin films, Appl. Phys. Lett. 84 (2004) 5255.

[9] S. Singh, N. Rama, K. Sethupathi, M.S. Ramachandra Rao, Correlation between electrical transport, optical, and magnetic properties of transition metal ion doped ZnO, J. Appl. Phys. 103 (2008) 07D108.

ACCEPTED MANUSCRIPT

[10] T. Kaspar, J. Fiedler, I. Skorupa, D. Bürger, A. Mücklich, M. Fritzsche, O.G. Schmidt, H. Schmidt, Persistent current reduction in metal semiconductor FETs with a ZnCoO channel in an external magnetic field, IEEE Electron Device Letters 34 (2013) 1271-1273.

[11] T. Kaspar, J. Fiedler, I. Skorupa, D. Bürger, O.G. Schmidt, H. Schmidt, Transport in ZnCoO thin films with stable bound magnetic polarons, APL Mat. 2 (2014) 076101.

[12] B. Pandey, S. Ghosh, P. Srivastava, P. Kumar, D. Kanjilal, S. Zhou, H. Schmidt, Room temperature transparent ferromagnetism in 200 keV Ni^{2+} ion implanted pulsed laser deposition grown ZnO/sapphire film, J. Appl. Phys. 107 (2010) 023901.

[13] H. Liu, F. Zeng, S. Gao, G. Wang, C. Song, F. Pan, Contributions of magnetic properties in epitaxial copper doped ZnO, Phys. Chem. Chem. Phys. 15 (2013) 13153.

[14] M. Ivill, S.J. Pearton, S. Rawal, L. Leu, P. Sadik, R. Das, A.F. Hebard, M. Chisholm, J.D. Budai, D.P. Norton, Structure and magnetism of cobalt doped ZnO thin films, New J. Phys. 10 (2008) 065002.

[15] J.H. Kim, H. Kim, D. Kim, Y.E. Ihm, W.K. Choo, Magnetic properties of epitaxially grown semiconducting $Zn_{1-x}Co_xO$ thin films by pulsed laser deposition, J. Appl. Phys. 92 (2002) 6066-6071.

[16] M. Venkatesan, P. Stamenov, L.S. Dorneles, R.D. Gunning, B. Bernoux, J.M.D. Coey, Magnetic, magnetotransport, and optical properties of Al doped $Zn_{0.95}Co_{0.05}O$ thin films, Appl. Phys. Lett. 90 (2007) 242508.

[17] S.M. Heald, T. Kaspar, T. Droubay, V. Shutthanandan, S. Chambers, A. Mokhtari, A.J. Behan, H.J. Blythe, J.R. Neal, A.M. Fox, G.A. Gehring, X ray absorption fine structure and magnetization characterization of the metallic Co component in Co doped ZnO thin films, Phys. Rev. B 79 (2009) 075202.

ACCEPTED MANUSCRIPT

[18] H.S. Hsu, J.C.A. Huang, Y.H. Huang, Y.F. Liao, M.Z. Lin, C.H. Lee, J.F. Lee, S.F. Chen, L.Y. Lai, C.P. Liu, Evidence of oxygen vacancy enhanced room-temperature ferromagnetism in Co doped ZnO, Appl. Phys. Lett. 88 (2006) 242507.

[19] A.J. Behan, A. Mokhtari, H.J. Blythe, D. Score, X.H. Xu, J.R. Neal, A.M. Fox, G.A. Gehring, Two magnetic regimes in doped ZnO corresponding to a dilute magnetic semiconductor and a dilute magnetic insulator, Phys. Rev. Lett. 100 (2008) 047206.

[20] J.M.D. Coey, M. Venkatesan, C.B. Fitzgerald, Donor impurity band exchange in dilute ferromagnetic oxides, Nature Mater. 4 (2005) 173-179.

[21] J. Alaria, H. Bieber, S. Colis, G. Schmerber, A. Dinia, Absence of ferromagnetism in Al doped $Zn_{0.9}Co_{0.10}O$ diluted magnetic semiconductors, Appl. Phys. Lett. 88 (2006) 112503.

[22] T.C. Kaspar, T. Droubay, S.M. Heald, P. Nachimuthu., C.M. Wang, V. Shutthanandan, C.A. Johnson, D.R. Gamelin, S.A. Chambers, Lack of ferromagnetism in n-type cobalt doped ZnO epitaxial thin films, New J. Phys. 10 (2008) 055010.

[23] Z.L. Lu, H.S. Hsu, Y.H. Tzeng, F.M. Zhang, Y.W. Du, J.C.A. Huang, The origins of ferromagnetism in Co doped ZnO single crystalline films: From bound magnetic polaron to free carrier mediated exchange interaction, Appl. Phys. Lett. 95 (2009) 102501.

[24] B. Pandey, S. Ghosh, P. Srivastava, P. Kumar, D. Kanjilal, Influence of microstructure on room temperature ferromagnetism in Ni implanted nanodimensional ZnO films, J. Appl. Phys. 105 (2009) 033909.

[25] P. Satyarthi, S. Ghosh, P. Mishra, B.R. Sekhar, F. Singh, P. Kumar, D. Kanjilal, R.S. Dhaka, P. Srivastava, Defect controlled ferromagnetism in xenon ion irradiated zinc oxide, J. Mag. Magn. Mater. 385 (2015) 318-325.

[26] J.M.D. Coey, d^0 ferromagnetism, Solid State Sciences 7 (2005) 660-667.

ACCEPTED MANUSCRIPT

[27] S.B. Singh, Y.F. Wang, Y.C. Shao, H.Y. Lai, S.H. Hsieh, M.V. Limaye, C.H. Chuang, H.C. Hsueh, H. Wang, J.W. Chiou, H.M. Tsai, C.W. Pao, C.H. Chen, H.J. Lin, J.F. Lee, C.T. Wu, J.J. Wu, W.F. Pong, T. Ohigashi, N. Kosugi, J. Wang, J. Zhou, T. Regier, T.K. Sham, Observation of the origin of d^0 magnetism in ZnO nanostructures using x-ray based microscopic and spectroscopic techniques, Nanoscale 6 (2014) 9166-9176.

[28] P. Satyarthi, S. Ghosh, Y.T. Wang, S. Zhou, P. Kumar, D. Kanjilal, L. Olivi, D. Bürger, I. Skorupa, H. Schmidt, P. Srivastava, Probing defect driven tunable spontaneous magnetization in paramagnetic $Zn_{0.95}Co_{0.05}O$ epitaxial films by x-ray absorption investigations, J. Alloys Comp. 649 (2015) 891-898.

[29] P. Satyarthi, S. Ghosh, Y. Wang, S. Zhou, D. Bürger, I. Skorupa, H. Schmidt, L. Olivi, P. Srivastava, Direct evidence of defect coordination and magnetic interaction in local structure of wurtzite type Zn1-xCoxO thin films, J. Alloys Comp. 670 (2016) 113-122.

[30] P. Kumar, G. Rodrigues, D. Kanjilal, A. Roy, B.P. Singh, R. Kumar, Development of Zn and Eu beams by plasma sputtering, Nucl. Instrum. Methods Phys. Res. B 246 (2006) 440-444.

[31] J.F. Ziegler, J.P. Biersack, U. Littmark, The Stopping Power of Ions in Solids, Pergamon, New York, 1980.

[32] C.D. Wagner, W.M. Riggs, L.E. Davis, J.F. Moulder, G.E. Muilenberg, Handbook of X-ray Photoelectron Spectroscopy, Perkin Elmer, Eden Prairie, pp. 80 and 84, 1979.

[33] M.N. Islam, T.B. Ghosh, K.L. Chopra, H.N. Acharya, XPS and X- ray diffraction studies of aluminum doped zinc oxide transparent conducting films, Thin Solid Films 280 (1996) 20-25.

[34] P. Srivastava, S. Ghosh, B. Joshi, P. Satyarthi, P. Kumar, D. Kanjilal, D. Buerger, S. Zhou, H. Schmidt, A. Rogalev, F. Wilhelm, Probing origin of room temperature ferromagnetism in Ni ion implanted ZnO films with x-ray absorption spectroscopy, J. Appl. Phys. 111 (2012) 013715.

ACCEPTED MANUSCRIPT

[35] P. Satyarthi, S. Ghosh, B. Pandey, P. Kumar, C.L. Chen, C.L. Dong, W.F. Pong, D. Kanjilal, K. Asokan, P. Srivastava, Coexistence of intrinsic and extrinsic origins of room temperature ferromagnetism in as implanted and thermally annealed ZnO films probed by x-ray absorption spectroscopy, J. Appl. Phys. 113 (2013) 183708.

[36] J.C.C. Fan, J.B. Goodenough, X-ray photoemission spectroscopy studies of Sn doped indium oxide films, J. Appl. Phys. 48 (1977) 3524.

[37] M. Chen, X. Wang, Y.H. Yu, Z.L. Pei, X.D. Bai, C. Sun, R.F. Huang, L.S. Wen, X-ray photoelectron spectroscopy and auger electron spectroscopy studies of Al doped ZnO films, Appl. Surf. Sci. 158 (2000) 134-140.

[38] H. Chou, C.P. Lin, J.C.A. Huang, H.S. Hsu, Magnetic coupling and electric conduction in oxide diluted magnetic semiconductors, Phys. Rev. B 77 (2008) 245210.

[39] H. Chou, C.P. Lin, H.S. Hsu, S.J. Sun, The role of carriers in spin current and magnetic coupling for ZnO:Co diluted magnetic oxides, Appl. Phys. Lett. 96 (2010) 092503.

[40] M. Yu, H. Qiu, X. Chen, Effect of vacuum magnetic annealing on the structural and physical properties of the Ni and Al co doped ZnO films, Thin Solid Films 518 (2010) 7174–7182.

[41] B. Joshi, S. Ghosh, P. Srivastava, P. Kumar, D. Kanjilal, Correlation between electrical transport, microstructure and room temperature ferromagnetism in 200 keV Ni^{2+} ion implanted zinc oxide (ZnO) thin films, Appl. Phys. A 107 (2012) 393.

[42] G.Z. Xing, Y.H. Liu, Y.F. Tian, J.B. Yi, C.C. Lim, Y.F. Li, G.P. Li, D.D. Wang, B. Yao, J. Ding, Y.P. Feng, T. Wu, Defect-induced magnetism in undoped wide band gap oxides: Zinc vacancies in ZnO as n example, AIP ADVANCES 1 (2011) 022152.

ACCEPTED MANUSCRIPT

Figure Captions

FIG. 1. Zn 2p core level spectra of as deposited and post irradiated $Zn_{0.95}Co_{0.05}O$ films corresponding to different fluences of xenon ions (5×10^{14}, 1×10^{16}, 5×10^{16} and 1×10^{17} ions/cm^2).

FIG. 2. O 1s core level spectra of as deposited $Zn_{0.95}Co_{0.05}O$ film: inset of figure shows the variation in relative area of oxygen vacancy mediated peak in $Zn_{0.95}Co_{0.05}O$ films with increase in xenon ions fluence.

FIG. 3. Co 2p core level spectra of as deposited and post irradiated $Zn_{0.95}Co_{0.05}O$ films corresponding to different fluences of xenon ions (5×10^{14}, 1×10^{16}, 5×10^{16} and 1×10^{17} ions/cm^2).

FIG. 4. Optical transmittance spectra of as deposited and post irradiated $Zn_{0.95}Co_{0.05}O$ films corresponding to different fluences of xenon ions (5×10^{14}, 1×10^{16}, 5×10^{16} and 1×10^{17} ions/cm^2).

FIG. 5. The variation in resistivity (ρ), carrier concentration (n_c) and Hall mobility (μ) of as deposited and post irradiated $Zn_{0.95}Co_{0.05}O$ films corresponding to different fluences of xenon ions (5×10^{14}, 1×10^{16}, 5×10^{16} and 1×10^{17} ions/cm^2).

FIG. 6. Resistivity versus temperature dependence of irradiated $Zn_{0.95}Co_{0.05}O$ films corresponding to fluences of 1×10^{16} and 5×10^{16} ions/cm^2.

FIG. 7. The Arrhenius plots of irradiated $Zn_{0.95}Co_{0.05}O$ films corresponding to fluences of 1×10^{16} and 5×10^{16} ions/cm^2 showing thermally activated band and NNH conduction.

FIG. 8. The $\ln(\sigma T^{1/2})$ versus $T^{-1/4}$ for irradiated $Zn_{0.95}Co_{0.05}O$ films corresponding to fluences of 1×10^{16} and 5×10^{16} ions/cm^2 showing VRH conduction.

FIG. 9. (a) The room temperature saturation magnetization and carrier concentration plotted as a function of fluence for irradiated $Zn_{0.95}Co_{0.05}O$ films (b) Comparison of room and low

temperature (5 K) *M-H* curves for irradiated $Zn_{0.95}Co_{0.05}O$ films corresponding to fluences of 1×10^{16} and 5×10^{16} ions/cm^2.

FIG. 10. Illustration of concentric BMPs spheres model in three limiting cases (i) perfect insulting (ii) Insulating, and (iii) Intermediate. The small solid circle (light blue) represents BMPs formation of radius r_{BMP} with respect to defects and substituted Co^{2+} ions. The large dotted sphere shows the VRH spheres with localization radius (r_{VRH}) around the defect. *R* represents the hopping distance of an electron between VRH spheres.

Table 1. The calculated values of Motts's variable range hopping parameters for irradiated $Zn_{0.95}Co_{0.05}O$ films corresponding to 1×10^{16} and 5×10^{16} ions/cm^2 fluences.

ACCEPTED MANUSCRIPT

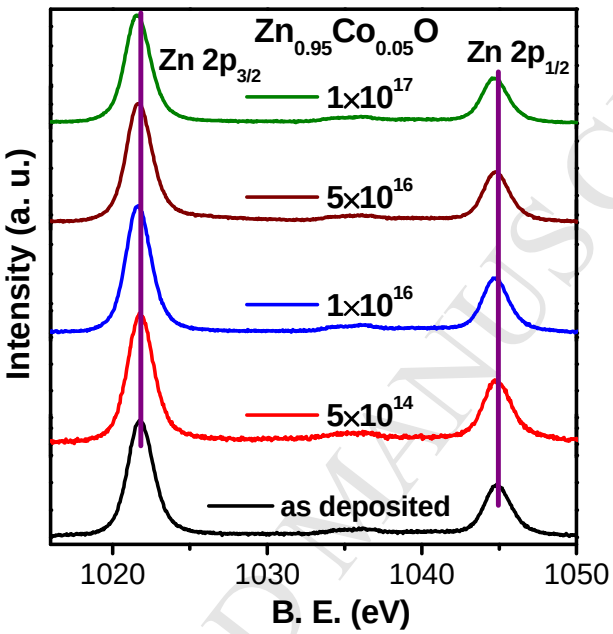

FIG. 1

ACCEPTED MANUSCRIPT

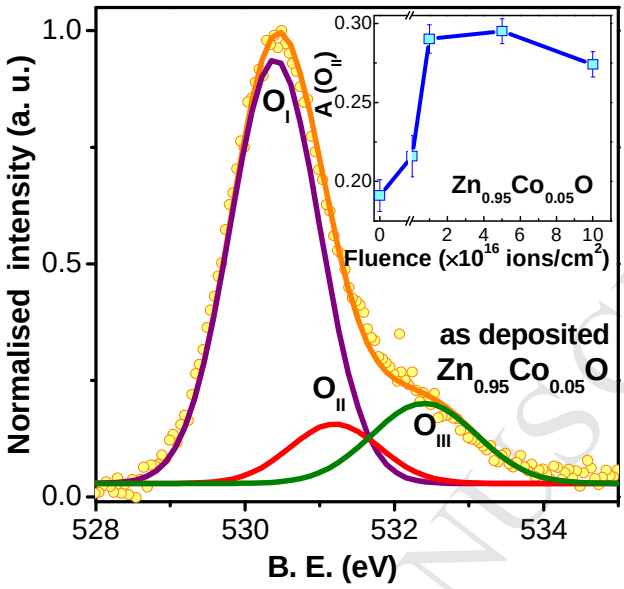

FIG. 2

ACCEPTED MANUSCRIPT

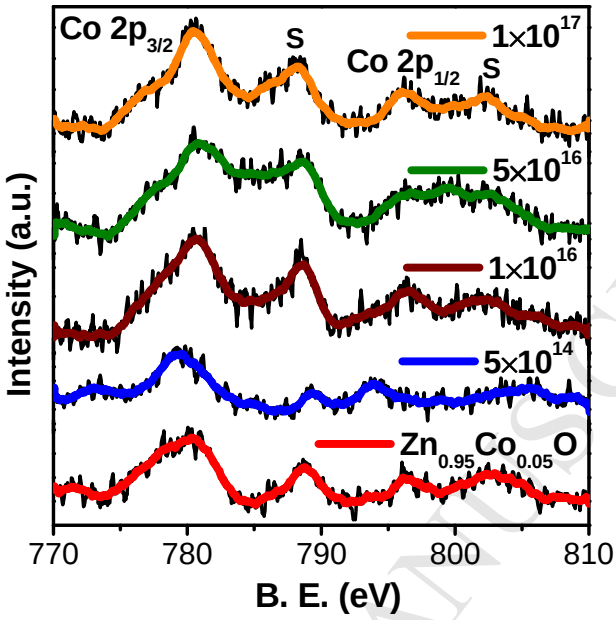

FIG. 3

ACCEPTED MANUSCRIPT

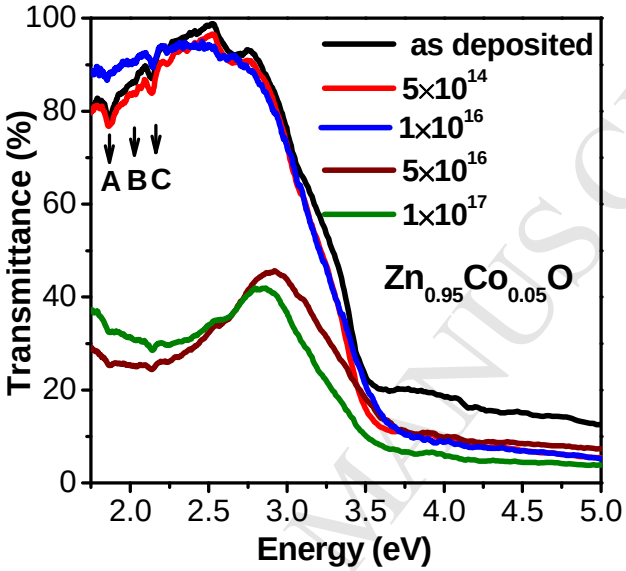

FIG. 4

ACCEPTED MANUSCRIPT

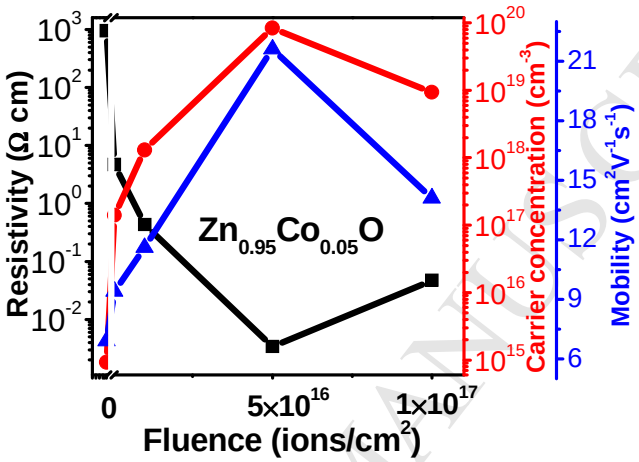

FIG. 5

ACCEPTED MANUSCRIPT

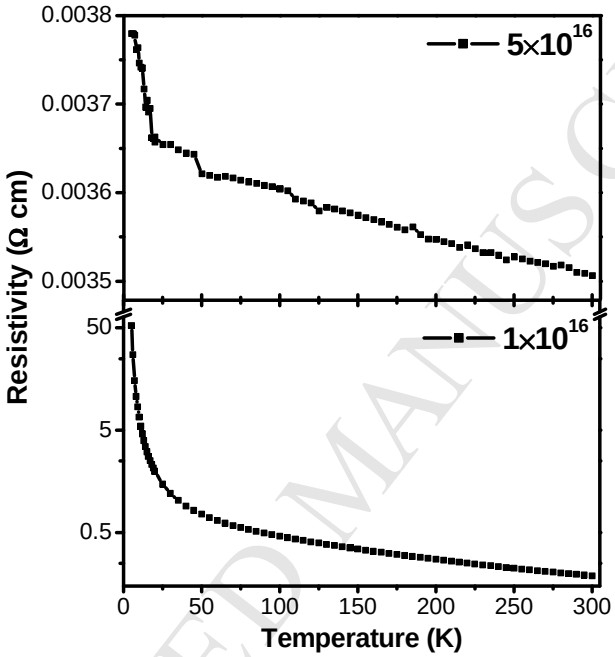

FIG. 6

ACCEPTED MANUSCRIPT

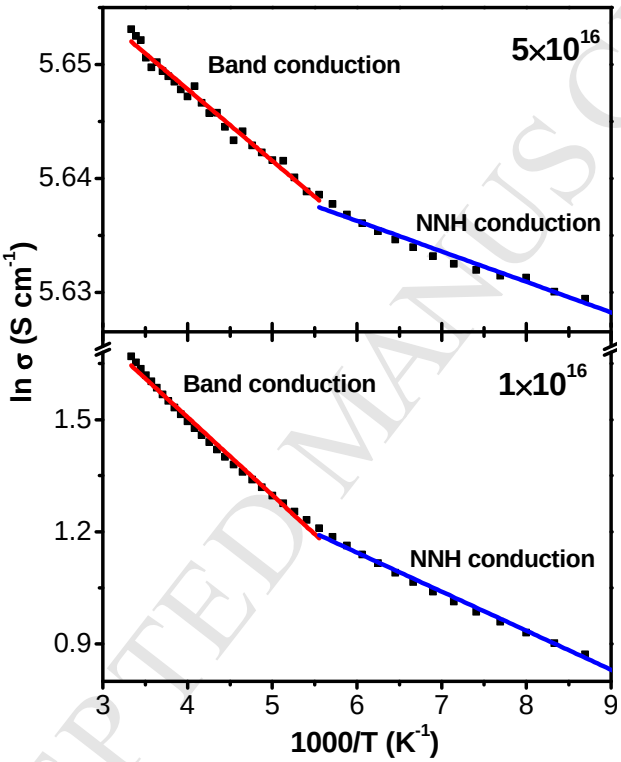

FIG. 7

ACCEPTED MANUSCRIPT

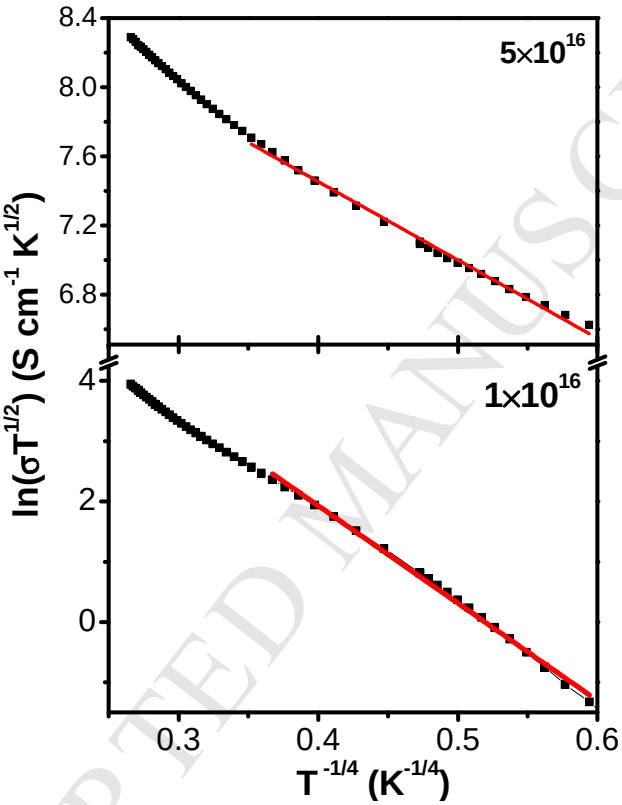

FIG. 8

ACCEPTED MANUSCRIPT

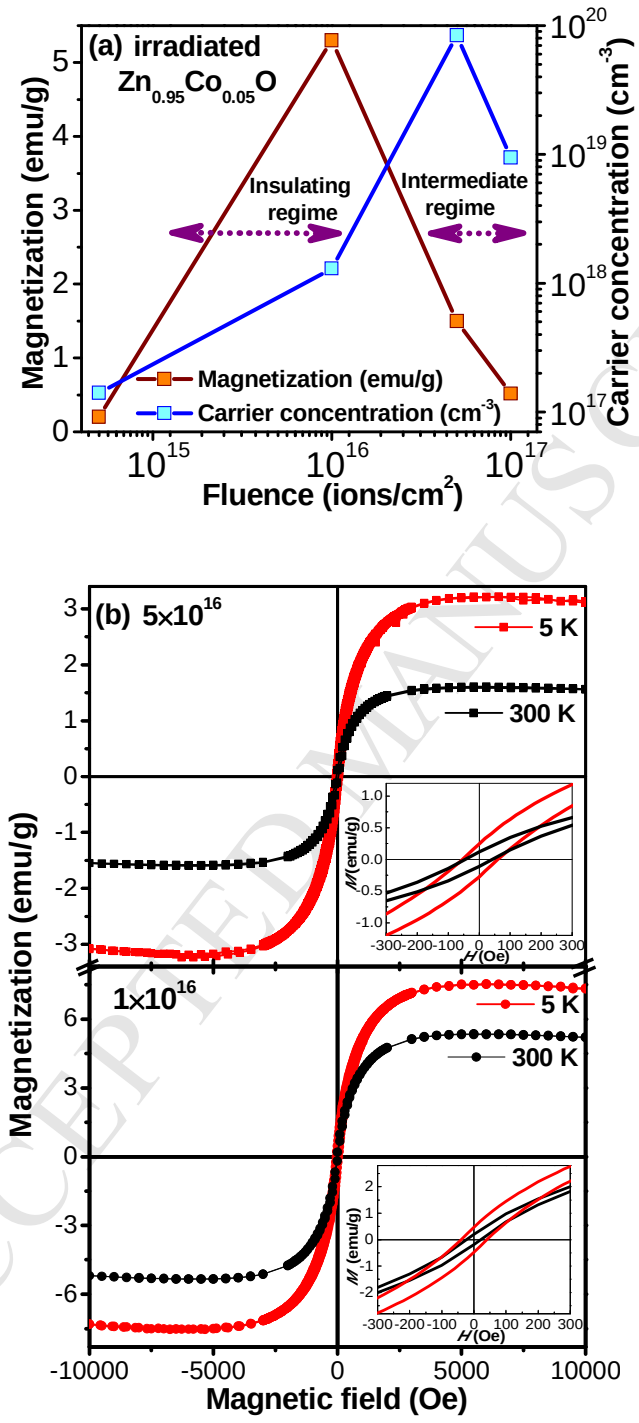

FIG. 9

ACCEPTED MANUSCRIPT

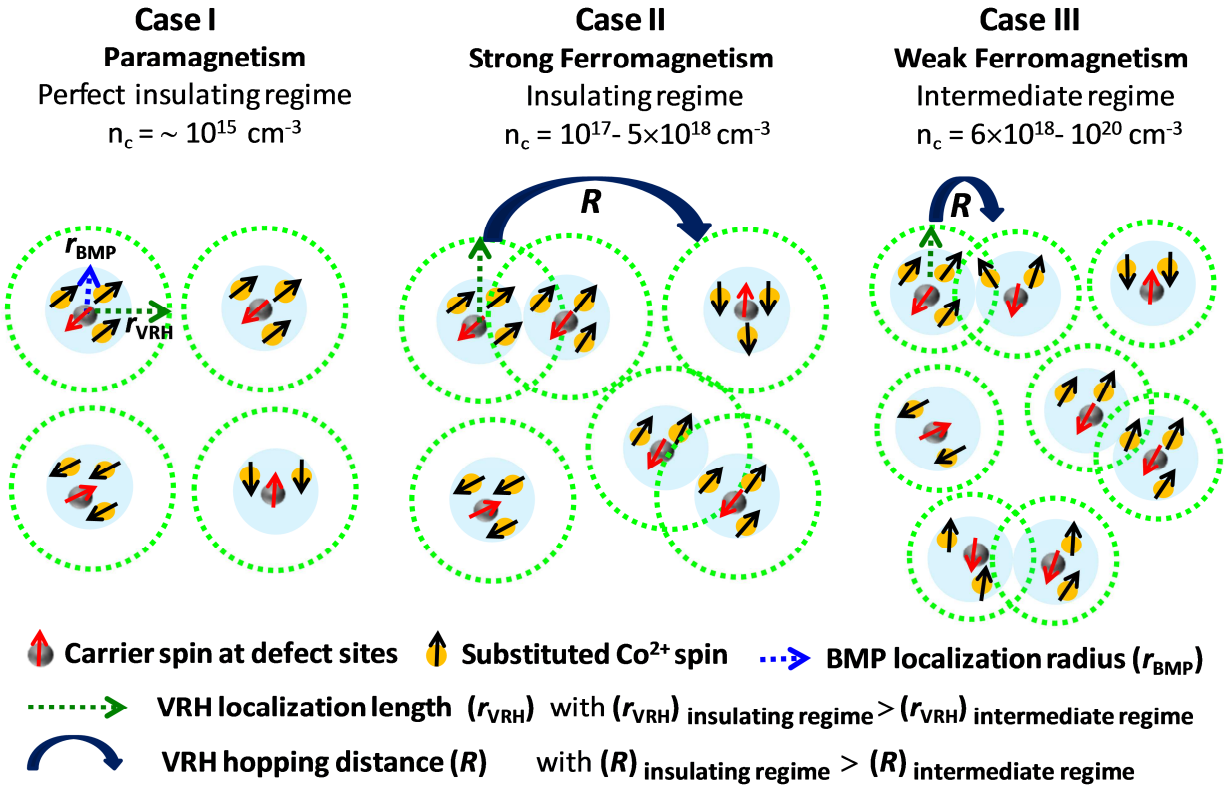

FIG. 10

ACCEPTED

Table 1. The calculated values of Motts's variable range hopping parameters for irradiated $Zn_{0.95}Co_{0.05}O$ films corresponding to 1×10^{16} and 5×10^{16} ions/cm^2 fluences.

Irradiated $Zn_{0.95}Co_{0.05}O$ films	T_0 (K)	α (cm^{-1})	$N(E_F)$ (cm^{-3}eV^{-1})	r_{VRH} (nm)	R (nm)
1×10^{16} ions/cm^2	68000	4.3×10^{7}	2.2×10^{17}	23	52
5×10^{16} ions/cm^2	422	1.5×10^{6}	1.6×10^{21}	6.5	4

ACCEPTED MANUSCRIPT

ACCEPTED MANUSCRIPT

Highlights

- Transparent conducting and ferromagnetic properties are tuned in $Zn_{1-x}Co_xO$.
- Role of carrier's kinetics at variable temperatures is explored for understanding the ferromagnetism in transparent $Zn_{1-x}Co_xO$.
- The origin of ferromagnetism is explained from concentric bound magnetic polarons stabilization inside the variable range hopping spheres.
- The presence of strongly/weakly localized carriers is favourable/detrimental to ferromagnetism.

ACCEPTED MANUSCRIPT